Quantum Chaos In Semiconductor Structures

by Philip Peter Rushton

Department of Physics

University of Durham

4H Theoretical dissertation, April 1999

The mathematician plays a game in which he himself invents the rules while the physicist plays a game in which the rules are provided by Nature, but as time goes on it becomes increasingly evident that the rules which the mathematician finds interesting are the same as those which Nature has chosen.

Paul Adrien Maurice Dirac

Abstract

Investigation of the 3-dimensional classical motion of an electron confined between infinitely high parallel potential barriers is carried out, with a uniform electric field applied normal to the barriers and a magnetic field applied at an angle θ to the planar barriers. Analysis shows that tilting the magnetic field away from the normal induces a transition from regular motion ($\theta = 0°$) to strongly chaotic motion ($\theta \neq 0°$). The potential well is 120 nm-wide and so is sufficiently small that quantum mechanical calculations may be undertaken.

In the tilted magnetic field regime, the majority of the energy eigenstates reveal complex probability density patterns of maxima and minima, randomly distributed throughout the well. There also occur individual eigenstates, separated at fairly regular energy intervals that display a strikingly clear channel of enhanced probability density across the well. The region of increased probability density is shown to exist around a particular set of electron trajectories that continually repeat the same path throughout the well. This remarkable phenomenon is termed 'scarring' of the electron wavefunction and provides a definite link between chaos in classical and quantum mechanics.

Contents

1 Introduction **4**

2 The origin of chaos in classical Hamiltonian systems **9**

2.1 Introduction 9

2.2 Integrable Systems 11

2.3 Non-Integrability, Chaos and the KAM Theorem 11

2.4 Surfaces of Section 12

3 Theoretical predictions of scarred quantum wavefunctions **15**

4 Classical orbits and quantum mechanical states in a trapezoidal potential well in a tilted magnetic field **17**

4.1 Description of the system 17

4.2 Classical mechanics of the system 17

4.2.1 Classical orbits inside the potential well 18

4.2.2 The collision process at a potential barrier 20

4.2.3 Obtaining classical periodic orbits of the system 22

4.3 The Quantum Mechanics of the System 23

4.3.1 Stationary states in quantum mechanics 23

4.3.2 Quantum eigenstates of the potential well 24

5 Results **27**

5.1 Classical motion of an electron in a magnetic field applied at $\theta = 0°$ 27

5.2 Classical motion of an electron in a magnetic field applied at $\theta = 20°$ . . . 28

5.3 Quantum wavefunctions of the well in the tilted magnetic field regime . . . 34

6 Discussion **43**

7 Conclusion **45**

A Program Listings **46**

References **50**

Chapter 1

Introduction

The study of 'quantum chaos' seeks to discover the connection between classically chaotic systems and the corresponding description of such systems given by quantum mechanics. The correspondence principle was introduced by Niels Bohr in 1923 to describe classical mechanics as an approximation to quantum mechanics in the appropriate limit. However he quickly realised that it could only be applied to regular systems and hence fully or even partially chaotic systems avoided any description in the quantum regime. It is only quite recently that progress has been made in understanding the general framework that underlies this research field.

The characteristic features of chaos, i.e. sensitivity to initial conditions and deterministic unpredictability are only applicable to classical dynamical systems. This is because the exponential divergence of nearby states that are characteristic of classical chaos are suppressed in quantum mechanics, owing to the linear nature of the time-dependent Schrödinger equation. It is also stated that the smooth wavefunctions of quantum mechanics cannot possibly describe the infinitely detailed structure of irregular paths made by bodies executing chaotic motion. These ideas lead one to believe whether chaos can exist at all in quantum mechanics.

Exponential divergence of neighbouring states is only one aspect of classical chaos, and thankfully not the whole story. Since the advent of faster and more powerful computers, numerical techniques have allowed more sense to be made of the complex patterns of trajectories exhibited by chaotic systems that otherwise seemed impossible to analyse. Subsequent examination of the 'sea' of chaotic paths reveals special types of paths known as 'periodic orbits'. Instead of moving completely randomly throughout space, periodic orbits move along distinct closed orbits that continually retrace the same path at each cycle. They are difficult to locate because of their small number and their instability to tiny perturbations.

The earliest studies of quantum chaos concentrated on the statistical distribution of

energy levels of chaotic spectra. Paradoxically, the energy levels of a non-chaotic quantum system are distributed randomly whereas the energy levels of a chaotic quantum system exhibit strong regularity and appear to have strong links with periodic orbits. This was demonstrated by Friedrich and Wintgen (1989) in experimental investigations of absorption spectra of highly excited hydrogen atoms in strong magnetic fields. The absorption of radiation appeared to be random at near-ionisation energies, however Fourier analysis showed that the well separated peaks of the transformed spectrum correspond precisely to one of several standard periodic orbits of the classical system.

Previous to this, work by Gutzwiller (1970) showed that the quantum mechanical spectrum of a classically chaotic system could be accurately described in terms of a complete set of classical periodic orbits. Consequently his deductions on periodic orbit theory, which are confirmed by experiment, have played a crucial role in deriving the statistical properties of chaotic quantum spectra.

More recently, attention has turned to the eigenfunctions associated with the energy levels of quantum systems. A favourite model that has been studied extensively is that of a free particle motion confined within a stadium shaped boundary called a Bunimovich stadium, see figure 1. It is from a class of models known as 'quantum billiards' since a particle moves in straight lines on a two-dimensional plane unless it collides with the hard boundary. In this instance the particle undergoes an elastic reflection, reversing the momentum perpendicular to the boundary wall. The classical system was shown by Bunimovich (1979) to be strongly chaotic with a typical trajectory quickly covering most of the available ground inside the stadium in a complex way.

Such behaviour suggests that the probability density distribution of the particle for the analogous quantum system would similarly look random and irregular. Indeed this was found to be the case for most eigenstates. However theoretical calculations predicted significant differences between the eigenfunctions of the system which had profound implications on existing ideas on chaotic wavefunctions. Heller (1984) proved that a small set of individual eigenstates in the Bunimovich stadium display intensity patterns with distinct linear regions of enhanced probability density, which he called "scars". More

importantly the scars appeared to converge around unstable classical periodic orbits of the system as shown in figure 2. Therefore the periodic orbits that were used to unravel the nature of energy levels also play a fundamental role in the corresponding eigenfunctions. These results gave new implications for periodic-orbit theory and their importance in quantum chaos.

Advances in semiconductor micro-fabrication have meant that electron transport in mesoscopic devices is effectively 'ballistic' owing to the fact that impurity scattering can be neglected and also the mean free path of electrons exceeds the size of the microstructure. Hence, only scattering from the precisely formed boundaries of the device are important. This allows quantum mechanical transport through the device to be compared with classical 'billiard ball' type experiments where electrons are considered as classical balls that elastically bounce off the confining sidewalls. These systems therefore provide an ideal basis for studying the correspondence between classically chaotic systems and the corresponding description in quantum mechanics.

The first conclusive evidence for quantum scarring that confirm quantum mechanical predictions, came from experiments on electron transport in a semiconductor device called a resonant tunnelling diode (RTD), see Fromhold (1995). This device consists of a quantum well (approximately 100 nm-wide) made from GaAs/AlGaAs materials. In the RTD the well walls are grown flat to the precision of one or two atomic layers. Electrons tunnel into the well and move subject to an electric field applied perpendicular to the well walls. The electrons perform ballistic scattering events with the side walls of the well which coupled with a tilted magnetic field provides a classically chaotic system. The RTD is an extremely useful device for analysing the quantum signatures of a classically chaotic system since the electron states in the well can be experimentally probed by measuring the current–voltage characteristics that occur due to the tunnelling of the electrons.

Experimental measurements confirmed quantum mechanical predictions by Wilkinson (1997) that some of the energy eigenstates of the RTD were 'scarred', in that the majority of the current through the device was carried by electrons moving along scarred paths; which are also classical periodic orbits of the system. This project studies a simple model

that is reminiscent of the quantum well used in the RTD in an attempt to observe scarred wavefunctions of a quantum system that is shown to be strongly chaotic in the classical regime.

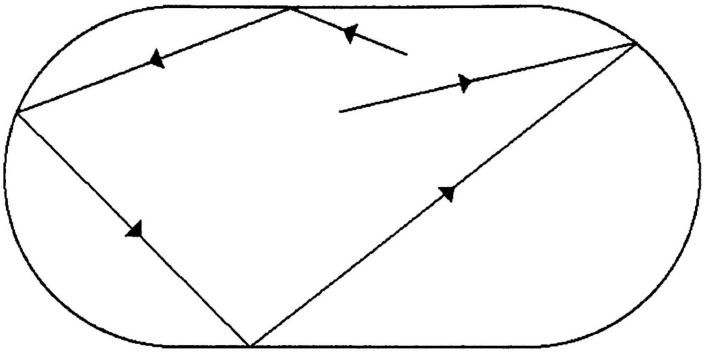

Figure 1: Classical trajectory of a particle moving inside a Bunimovich stadium.

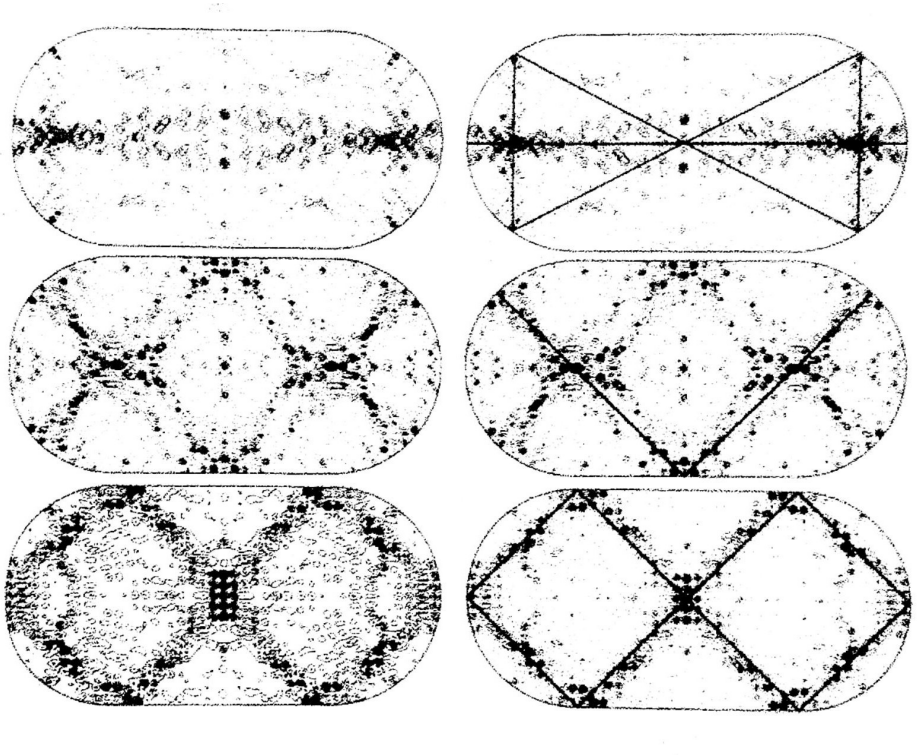

Figure 2: Left column, three probability density plots of scarred eigenstates of the Bunimovich billiard stadium. The right column illustrates how the probability density is enhanced along the trajectory of specific unstable periodic orbits shown overlaid. (After, Heller, 1984)

Chapter 2

The origin of chaos in classical Hamiltonian systems

2.1 Introduction

Classical dynamical systems may be grouped into three different classes. The first contains systems with regular, predictable motion as found in standard textbooks on classical mechanics (see for example Goldstein, 1992). At the other extreme are the completely chaotic systems. For these systems nearby trajectories diverge exponentially giving the appearance of random and complex behaviour, despite the deterministic equations that describe them. The third category comprises a mixture of both types of dynamics and is by far the most commonly found in nature out of the three classes. Systems that conserve energy are known as Hamiltonian systems. The time evolution of regular, non-chaotic systems is most easily described using Hamilton's equations of motion, which also provides a basis for understanding chaotic phenomenon. The Hamiltonian formulation has the added advantage that it can be used to analyse other completely unrelated systems. An important example of which is the Hamiltonian structure of quantum mechanics.

The general mathematical formulation of Hamiltonian dynamics is as follows: a system with N degrees of freedom is defined in terms of generalised co-ordinates q_i, of the position vector $\mathbf{q}$, conjugate momenta p_i, of the canonical momentum vector $\mathbf{p}$, $(i = 1, \ldots, N)$ and an energy function $H(p_i, q_i)$, known as the Hamiltonian for the system. The Hamiltonian completely specifies the dynamics, giving also the total conserved energy E, of the system. The equations of motion for the system are derived from $H(p_i, q_i)$ using Hamilton's equations

$$\frac{dp_i}{dt} = -\frac{\partial H}{\partial q_i} \tag{2.0.a}$$

$$\frac{dq_i}{dt} = \frac{\partial H}{\partial p_i} \tag{2.0.b}$$

The state of a dynamical system, at a given instant of time, is described using a phase space construction formed by the set of generalised co-ordinates and conjugate momenta, $\{q_i\}$ and $\{p_i\}$, respectively. This results in a 2N-dimensional space. Since energy is conserved, there is one less degree of freedom for the system (also known as a constant of the motion) and a given trajectory will therefore move in a space of $2N-1$ dimensions. Any other constants of motion (conserved quantities for the system) will similarly restrict the number of degrees of freedom. A classical trajectory, in a system with energy as the sole conserved quantity, therefore moves along a $2N-1$ dimensional surface in phase space, accessing only the regions for which the state $(\mathbf{p}, \mathbf{q})$ of the system is consistent with the value of E for the motion. It can be shown (see Arnold, 1978) that every trajectory moves along a surface in the shape of an N-dimensional torus, an example of which is shown in figure 3. The trajectories of the system move on individual tori that are nested within each other. The next two sections describe both regular and chaotic dynamics in terms of these tori and the reasons why chaos is generated in classical mechanical systems.

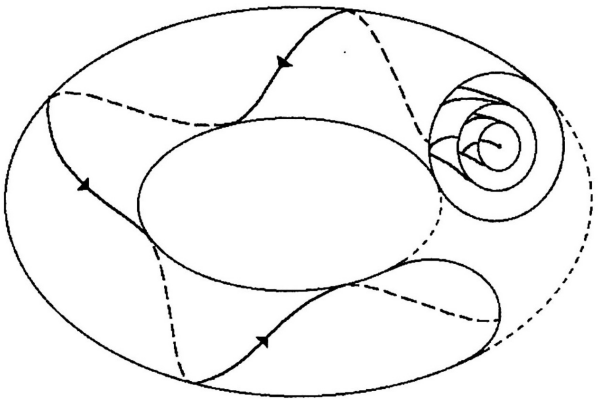

Figure 3: Representation of classical trajectories in three-dimensional phase space. Conservation of energy means that trajectories are confined to move along the two-dimensional surfaces of nested tori.

2.2 Integrable Systems

A system that exhibits regular (textbook) motion is called an integrable system. A Hamiltonian system is said to be completely integrable if there exist as many independent constants of motion as there are degrees of freedom. For motion about a given torus, there exist characteristic frequencies of the motion ω_i $(i = 1, \ldots, N-1)$. The frequencies vary for each torus and are determined by the constants of motion for the stable system. The behaviour of a trajectory is determined by the value of the frequency ω_i for the particular torus on which it is confined to move. If the ratio between the frequencies is irrational then the motion on a given torus is quasi-periodic, i.e. the motion will never exactly repeat itself. If, however, the frequency ratios are all rational, the motion will eventually repeat on itself forming a closed trajectory known as a periodic orbit. Hence for a periodic orbit the trajectory will move around the torus returning to the same point in phase space for every 'revolution' of the torus.

The periodic orbits form a set of zero measure since although there are an infinite number of rational numbers, they are also infinitely outnumbered by the tori covered with quasi-periodic orbits. The next section describes the role played by periodic orbits in determining the properties of chaotic (non-integrable) systems.

2.3 Non-Integrability, Chaos and the KAM Theorem

Most systems in nature do not possess as many first integrals as degrees of freedom, consequently completely integrable systems occur in exceptional circumstances. Usually there exist perturbations that cause integrable systems to become chaotic. For a Hamiltonian system this is analogous to applying a perturbation, H_1 say, to an ordinary integral system H_0, that is

$$H = H_1 + \varepsilon H_0 \tag{1}$$

The degree of non-integrability is determined by the perturbation parameter ε. If a system becomes non-integrable, constraints are removed from the trajectories and they

begin to move more freely through phase-space, not necessarily confined to tori as in the integrable case. The effect of small perturbations on an integrable system is described by the Kolmogorov–Arnold–Moser (KAM) Theorem and provides a starting point for the understanding of the appearance of chaos in Hamiltonian systems (See Tabor 1989). The KAM Theorem states that for $\varepsilon \ll 1$, i.e. for weakly perturbed systems, tori with irrational ratios of the frequencies survive; these are called KAM tori, whilst tori with rational frequency ratios are destroyed. As the value of the perturbing parameter increases, KAM tori also start to breakup leading to more trajectories that are able to wander throughout all of phase-space constrained only by energy conservation. This transitionary regime presents a mixture of quasiperiodic (KAM) orbits, periodic orbits and chaotic trajectories co-existing within phase-space. In the strongly chaotic regime all of the KAM tori are destroyed however there still exist periodic orbits which are all unstable in character. The KAM theorem assures us that the transition from integrable to chaotic motion is not discontinuous. The degree of chaos in a system is defined in terms of the rate of divergence between pairs of orbits in phase-space and is measured in terms of Lyapunov exponents, λ_i. There exists one such exponent for each dimension in phase-space. If all the Lyapunov exponents are zero the motion is regular, however if even one is positive, the motion will be chaotic. This exponential divergence of initially close orbits gives the ubiquitous definition of chaos as the sensitive dependence of motion on the initial conditions.

2.4 Surfaces of Section

To help visualise trajectories moving along tori in multi-dimensional phase-space, a most valuable technique called a Poincaré section, or surface of section has been developed for this purpose and is the main tool for studying the dynamics of Hamiltonian systems.

The study of orbits for a given energy can be reduced from the $2N-1$ dimensions in phase-space to an easier two-dimensional representation by taking a 'slice' of the phase-space at some given point. This slice is known as a Poincaré section. The Poincaré section is generated by recording on the designated Poincaré section, the points at which a given trajectory intersects that surface as it proceeds along its designated path. The orbit will

repeatedly pass through this phase-space plane thus building up a 'map' of successive values, as illustrated in figure 4.

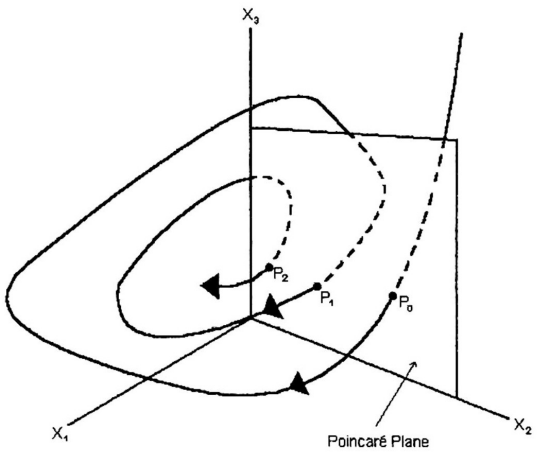

Figure 4: A Poincaré section (surface of section) for a three-dimensional phase space. The type of motion exhibited by a system is indicated by the manner in which the intersecting points P_0, P_1, P_2,... of a single trajectory accumulate on the Poincaré plane.

A periodic trajectory moving along a given tori would close smoothly on itself, consequently periodic motion is represented as a single point intersecting the Poincaré plane, figure 5a. If the motion is quasi-periodic and the ratio of frequencies is irrational, the Poincaré section will reveal a circular set of points as shown in figure 5b. As discussed in the previous section, the KAM theorem states that most invariant tori are preserved. Figure 5c illustrates a strongly chaotic phase in which the Poincaré section shows a random scatter of points due to the 'sea' of unconstrained chaotic orbits. The scattering of points is limited to a finite area due to energy conservation. When computed for a large number of initial conditions at the same energy, a Poincaré section is able to give an immediate picture of the complicated phase-space structure of a system.

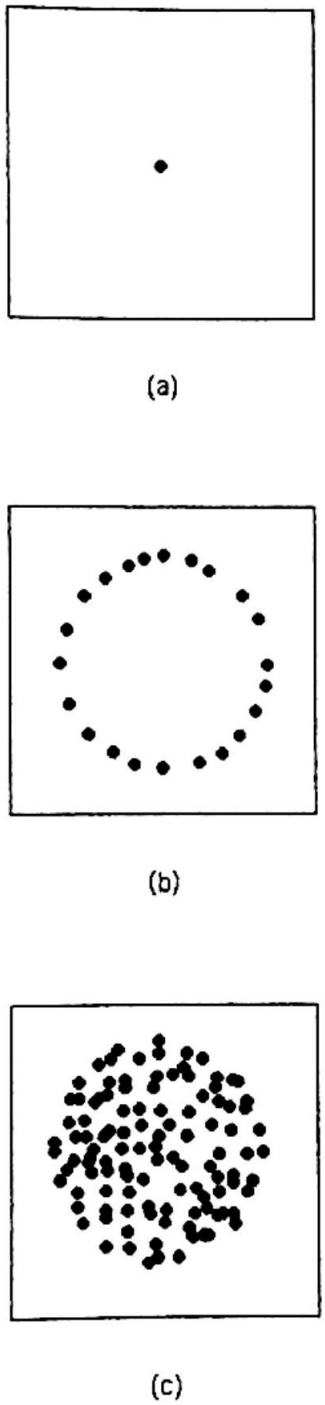

Figure 5: Poincaré sections showing the different types of motion found in classical dynamics. (a) A periodic orbit whereby the trajectory continually returns to the same point in phase space. (b) Quasi-periodic motion, and (c) randomly distributed points characteristic of motion that is strongly chaotic.

Chapter 3

Theoretical predictions of scarred quantum wavefunctions

The concern of this investigation is with the properties of individual eigenfunctions of a system which is known to be strongly chaotic in the classical regime. Phase-space in classically chaotic systems has infinitely detailed structure because of the unconstrained nature of the trajectories described in chapter 2. At the quantum level there cannot be this amount of detail in the wavefunctions since the uncertainty principle smooths out this detail. This raises the interesting question of what chaotic eigenfunctions look like and what is the underlying theory that predicts their nature.

The characteristic features of energy eigenfunctions of chaotic systems was proposed by Berry (1977) using a combination of classical and quantum ideas known as semiclassical mechanics. For quasi-periodic classical dynamics, quantum amplitudes in the semi-classical approximation are represented by

$$\Psi(x) = \sum_n \sqrt{P_n(x)}\, e^{iS_n(x)/\hbar} \tag{2}$$

since the motion is quasi-periodic there exist a finite number of distinct ways of arriving at an arbitrary point x. Consequently $P_n(x)$ is the classical probability for the nth path reaching the point x in phase-space. $S_n(x)$ is the classical action along the nth path reaching x. The sum over x is required since there may be more than one way of reaching x. For regular motion the theory is well understood using the semiclassical analysis. However difficulties arise when extending the theory to chaotic motion. This is because there is an infinite number of trajectories that can access a given region in phase-space which leads to an infinite number of terms in equation (2). Berry conjectured that the above equation still holds with the added assumption that the eigenfunctions are a superposition of an infinite number of plane waves, each with randomly distributed amplitudes, phases and directions. Therefore contour plots of wavefunctions were predicted to consist of random patterns of interference maxima and minima.

In general, numerical calculations of chaotic systems tended to support Berry's conjecture. However, in a seminal paper on billiard type dynamics in Bunimovich stadia, Heller (1984) showed that not all eigenstates of the system conform to Berry's original conjecture. Instead, certain eigenstates consisted not of random nodal patterns, but of regions with strongly enhanced probability density concentrated around narrow channels inside the stadium. Another consequence of this phenomenon, which Heller called 'scars' and would have fundamental implications on the theory, is that the scarring of the wavefunctions forms around certain classes of unstable classical periodic orbits (see figure 2). Despite knowing about unstable periodic orbits from the work by Gutzwiller (1971), the mathematical construction of Berry's eigenstates effectively excludes the influence of unstable periodic orbits. This exclusion was based on the fact that although densely populated in phase-space, the unstable periodic orbits are of total measure zero making it unlikely that they would have any appreciable effect on the eigenfunctions.

Chapter 4

Classical orbits and quantum mechanical states in a trapezoidal potential well in a tilted magnetic field

4.1 Description of the system

This chapter describes the methods used for calculating the motion of an electron in the classical and quantum mechanical regimes for an essentially simple reminiscent of the potential well used in the resonant tunnelling diode. The system consists of a 120-nm wide quantum well (QW) with infinitely high parallel walls with a uniform electric field, **F**, applied normal to the potential barriers. Figure 6 illustrates the trapezoidal potential energy profile formed by the application of the electric field as well as the co-ordinate system adopted for this investigation. The left and right-hand barriers are labelled emitter and conduction barriers respectively because of the relation with the RTD where electrons are emitted into the QW via the first barrier and are conducted out of the well through the second barrier. The effect of applying a large magnetic field, **B**, across the QW is investigated with regard to the classical motion and the corresponding quantum eigenstates for an electron moving inside the well.

As can be deduced from figure 6, the electron moves unconstrained in the y-z plane at constant energy subject to the electric and magnetic fields but is necessarily confined in the x-direction by the barrier walls. When the magnetic field is applied perpendicular to the barrier walls the electron exhibits non-chaotic, stable motion. Chaos is generated in this system by simply tilting the magnetic field at an angle relative to the barriers. Consequently chaotic electron motion inside the well is investigated here for the single case of a magnetic field tilted at an angle 20° to the barrier walls in the x-z plane.

4.2 Classical mechanics of the system

The equations that describe the motion of an electron inside the well with applied electric and magnetic fields are completely integrable. Chaotic motion is caused by the non-

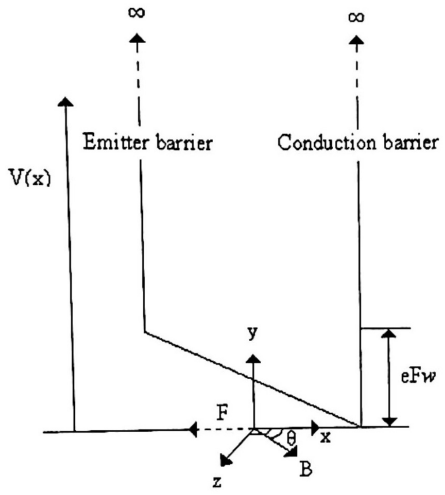

Figure 6: Profile of trapezoidal potential well and the co-ordinate system used in the analysis of electron motion inside the well. The origin of the co-ordinate system is situated at the centre of the well. The energy of the electron is taken with respect to the potential energy at the right-hand side of the well.

integrable nature of collisions with the potential barriers. In this case, one must resort to numerical methods in order to describe the state of the electron. An outline of how the analytical equations of motion between the barriers are obtained and how they are used to plot electron orbits inside the well is given first. The process of dealing with electron collisions with the barriers is described next concluding the classical analysis with a description of how periodic orbits of the system are found.

4.2.1 Classical orbits inside the potential well

An electron introduced into the potential well with effective mass m^* will experience a Lorentz force due to the applied electric field $\mathbf{F}$, and magnetic field $\mathbf{B}$, given by the standard equation

$$m^* \frac{d\mathbf{v}}{dt} = -e(\mathbf{F} + \mathbf{v} \times \mathbf{B}) \tag{3}$$

Since the magnetic field is tilted by an angle θ in the x-z plane, it can be represented as $\mathbf{B} = (B\cos\theta,\ 0,\ B\sin\theta)$ and the electric field applied across the well, $\mathbf{F} = (-F, 0, 0)$.

The components of velocity and position of the electron are determined by integrating

equation (3). It is easier to perform these integrations if the co-ordinate frame is rotated by an angle θ, about the y-axis so that the new axis, x', lies along the magnetic field direction (see figure 7). In this new co-ordinate system the components of velocity at time t, are given by:

$$\begin{aligned} v_{x'}(t) &= \frac{eF\cos\theta}{m^*}\,t + v_{x'}(0) \\ v_{y'}(t) &= (v_{y'}(0) - v_d)\cos\omega_c t - v_{z'}(0)\sin\omega_c t + v_d \\ v_{z'}(t) &= (v_{y'}(0) - v_d)\sin\omega_c t + v_{z'}(0)\cos\omega_c t \end{aligned} \tag{4}$$

where the components at $t = 0$ specify the initial velocity components as the electron first enters the well at the emitter barrier. The initial components must correspond exactly to the kinetic energy permitted by the total energy as measured at the right hand barrier.

Integrating the Lorentz force equation twice gives the electron position inside the well

$$\begin{aligned} x'(t) &= \frac{eF\cos\theta}{2m^*}\,t^2 + v_{x'}(0)t + x'(0) \\ y'(t) &= \frac{v_{z'}(t) - v_{z'}(0)}{\omega_c} + v_d t + y'(0) \\ z'(t) &= -\frac{v_{y'}(t) - v_{y'}(0)}{\omega_c} + z'(0) \end{aligned} \tag{5}$$

where $v_d = F\sin\theta/B$, corresponding to a drift velocity in the positive y'-direction. To plot electron orbits inside the well, the components of position in the unrotated system can be found in terms of the rotated components using the usual transformation equations

$$\begin{aligned} x &= x'\cos\theta - z'\sin\theta \\ y &= y' \\ z &= z'\cos\theta + x'\sin\theta \end{aligned} \tag{6}$$

similarly for the components of velocity. The electron trajectory is plotted throughout the well at time intervals of 1 picosecond.

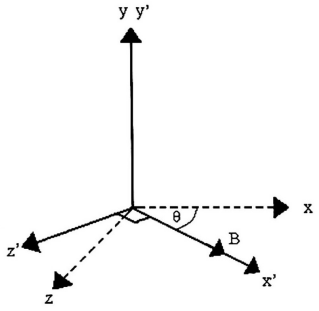

Figure 7: The rotated co-ordinate system used to calculate the classical electron trajectories inside the potential well.

4.2.2 The collision process at a potential barrier

Since energy is conserved throughout the motion, the electron makes elastic collisions with the confining barriers such that its velocity along the x-axis reverses while the components parallel to the barrier walls remain unchanged. The equations of motion are reset at the collision point with the new initial conditions and the electron reverses direction, moving now toward the opposite barrier. In order to determine the state of the electron as it collides with a barrier, and hence obtain new starting conditions, the time of the collision must be calculated. This will be given in terms of the time elapsed since the last collision with either barrier. Due to the irregular nature of the collisions and the inherent sensitivity of chaos, the time at which the electron collides with a barrier must be calculated as accurately as possible using a numerical technique. The method used here is as follows: when the electron is further than 6-nm away from either barrier the updating of the electron state proceeds as normal at each time step of 1 ps. When the electron approaches a barrier closer than 6-nm the time step is reduced to 0.01 ps in order to limit the time of collision to a smaller interval. A linear interpolation method is then used to determine the time of collision precisely.

Consider the electron colliding with the conduction barrier at $x = +1$ at time t_0 (the units are rescaled such that 60 nm = 1, therefore the emitter and conduction barriers are located at $x = -1$ and $x = +1$ respectively). The most recent calculation of the electron state before hitting the barrier is $(x(t_{n-1}),\ v(t_{n-1}))$, occurring at time t_{n-1}. Without

the barrier present the electron would continue on its path to the point $x(t_n)$ beyond the position of the barrier with velocity $v(t_n)$, at time t_n. The point of collision and therefore the time of collision t_0, must occur within this time interval. Therefore using linear interpolation we find that for a collision at the right-hand barrier, (see figure 8)

$$\frac{v_x(t_n) - v_x(t_{n-1})}{x(t_n) - x(t_{n-1})} = \frac{v_x(t_0) - v_x(t_{n-1})}{1 - x(t_{n-1})} \tag{7}$$

(substitute $x = -1$ for collisions with the emitter barrier). Rearranging this gives

$$v_x(t_0) = \left(\frac{v_x(t) - v_x(t_{n-1})}{x(t_n) - x(t_{n-1})}\right)\big(1 - x(t_{n-1})\big) + v_x(t_{n-1}) \tag{8}$$

using the above equation together with a similar expression for $v_z(t_0)$ yields $v_{x'}(t_0)$,

$$v_{x'}(t_0) = v_{x'}(t_0)\cos\theta + v_z(t_0)\sin\theta \tag{9}$$

and using equation (4.2a) we obtain the time of collision accurately as

$$t_0 = m^*\left(\frac{v_{x'}(t_0) - v_x(0)}{eF\cos\theta}\right) \tag{10}$$

The electron undergoes specular reflection with the barriers such that the velocity components before and after the collision are related by the condition, $v_x^a = -v_x^b$, $v_y^a = v_y^b$ and $v_z^a = v_z^b$. Therefore, only the x-component of velocity changes and the others remain unaltered. The state of the electron at the collision point is calculated by substituting t_0 into equations (4) and (5) which become the new starting conditions. The time parameter is then reset to zero and the process repeated for the return trajectory. Using the conditions of specular reflection, the new initial velocity components in the rotated co-ordinate system

become

$$\begin{aligned} v_{x'}(0) &= -v_x^b \cos\theta + v_z^b \sin\theta \\ v_{y'}(0) &= v_y^b \\ v_{z'}(0) &= v_z^b \cos\theta + v_x^b \sin\theta \end{aligned} \tag{11}$$

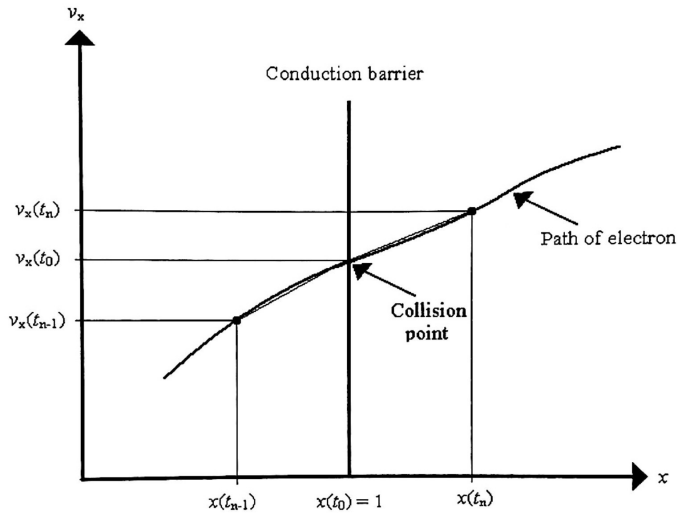

Figure 8: The interpolation method used to determine the velocity of the electron as it collides with the barrier. From this information, the time at which the electron collides with the barrier can be calculated and hence the new initial conditions are set for the return journey.

4.2.3 Obtaining classical periodic orbits of the system

Searching for periodic orbits in the QW is a matter of finding initial conditions for the equations of motion such that the electron continually returns to the same point. It may be shown [see Wilkinson (1997)] that if an electron returns to the emitter barrier with no change in the in-plane velocity components v_y, v_z then it also returns to the same position and the orbit is also a periodic orbit.

To locate a periodic orbit, a number of electron trajectories are initiated from the emitter barrier with velocity components $[v_x(0), v_y(0), v_z(0)]$ consistent with the energy at the right-hand barrier. When the electron returns to the emitter barrier the quantity

$\Delta = (\Delta v_y)^2 + (\Delta v_z)^2$ is evaluated. A periodic orbit will have $\Delta = 0$ hence initial velocity components are found such that Δ is reduced to a value $\leq 1 \times 10^{-8}$ and the trajectory is therefore in the neighbourhood of a periodic orbit. To obtain the periodic orbit more accurately the trajectory is plotted graphically and the initial velocity components are adjusted so that there are no visible deviations from periodicity after 40 periods and $\Delta = 0$ to within an accuracy of 1 part in 10^{10}.

4.3 The Quantum Mechanics of the System

4.3.1 Stationary states in quantum mechanics

The static electric and magnetic fields applied to the system lead to a time-independent Hamiltonian. Therefore to find the individual energy eigenstates E of an electron in the well, the stationary Schrödinger equation must be solved. That is

$$H(\hat{p}, q)\Psi(\mathbf{r}) = E\Psi(\mathbf{r}) \tag{12}$$

where the operator $\hat{p} = -i\hbar\nabla$. The most common method of numerical solution of this equation consists of expansion of the wavefunction $\Psi(\mathbf{r})$ in a series over a certain complete set of functions $\phi_n(\mathbf{r})$ with corresponding coefficients C_n

$$\Psi(\mathbf{r}) = \sum_{n}^{\infty} C_n \phi_n(\mathbf{r}) \tag{13}$$

Assuming $\phi_n(\mathbf{r})$ are orthogonal functions, the energy eigenvalues E_n and corresponding eigenvectors of the system can be calculated from the equation

$$\det\left|H_{n'n} - E_n I\right| = 0 \tag{14}$$

the Hamiltonian matrix elements are given by

$$H_{n'n} = \int \phi^*_{n'}(\mathbf{r})\, H(\hat{p}, \mathbf{r})\, \phi_n(\mathbf{r})\, d\mathbf{r} \tag{15}$$

The electron probability density distribution $P(E)$ is determined by evaluating the usual

relation

$$P(E) = \left|\Psi(\mathbf{r})\right|^2 \tag{16}$$

4.3.2 Quantum eigenstates of the potential well

The quantum mechanical Hamiltonian for an electron exposed to a magnetic field B, and potential energy $V(x)$, may be written in the standard form

$$H = \frac{1}{2m^*}\{\mathbf{p} + e\mathbf{A}\}^2 + V(x) \tag{17}$$

The magnetic field being specified by the vector potential, $\mathbf{B} = \nabla \times \mathbf{A}$. In this system the vector potential is chosen as $\mathbf{A} = (0,\, xB\sin\theta - zB\cos\theta,\, 0)$. Expanding the square $\{\hat{p} + e\hat{A}\}^2$, the Hamiltonian for the system becomes

$$H = \frac{1}{2m^*}\left\{p_x^2 + (p_y + exB\sin\theta - ezB\cos\theta)^2 + p_z^2\right\} + U(x) \tag{18}$$

where $U(x)$ is the trapezoidal potential produced by the electric field as shown in figure 10. The potential profile is given by

$$U(x) = \begin{cases} eF\left(\frac{1}{2}w - x\right) & |x| < \frac{1}{2}w \\ \\ \infty & |x| \geq \frac{1}{2}w \end{cases} \tag{19}$$

p_x, p_y, p_z are canonical momentum operators. The Hamiltonian is independent of the y co-ordinate, therefore p_y commutes with $\hat{H}$, i.e. the y component of the generalised momentum is conserved. Consequently we seek wavefunctions $\Psi_j(\mathbf{r})$, of the system in the form

$$\Psi_j(\mathbf{r}) = \chi_j(x,z)\, e^{i\left(\frac{p_y}{\hbar}\right)y} \tag{20}$$

$\chi_j(x,z)$ satisfies the 2-dimensional Schrödinger equation given by

$$\begin{aligned} H\chi_j(x,z) &= \left[\frac{1}{2m^*}\left\{p_x^2 + (p_y + exB\sin\theta - ezB\cos\theta)^2 + p_z^2\right\} + U(x)\right]\chi_j(x,z) \\ &= \varepsilon_j\,\chi_j(x,z) \end{aligned} \tag{21}$$

The basis states of $\Psi_j(\mathbf{r})$ can be expressed in the form

$$\Psi_j(\mathbf{r}) = \sum_{r,n} C_{r,n}^j\,\psi_r(x)\,\phi_n(z)\,e^{i\left(\frac{p_y}{\hbar}\right)y} \tag{22}$$

comprised of one-dimensional eigenfunctions, $\psi_r(x)$, of the potential $U(x)$ where ($r = 1, 2, 3\ldots$)

$$\psi_r(x) = \sqrt{\frac{2}{w}}\sin\!\left(\frac{\pi r\bar{x}}{w}\right) \tag{23}$$

and simple harmonic oscillator (SHO) eigenstates, $\phi_n(z)$, ($n = 0, 1, 2\ldots$).

$$\phi_n(\bar{z}) = \left(\frac{2m^*\omega_c\cos\theta}{\hbar}\right)^{\frac{1}{4}}\frac{1}{\sqrt{2^n n!}}\,e^{-\left(\frac{m^*\omega_c\cos\theta}{2\hbar}\right)\bar{z}^2}H_n\!\left(\bar{z}\left[\frac{m^*\omega_c\cos\theta}{\hbar}\right]^{\frac{1}{2}}\right) \tag{24}$$

where H_n is the nth Hermite polynomial, $\bar{x} = x + w/2$. Within this basis, the Hamiltonian reduces to a real symmetric banded matrix. The expansion coefficients $C_{r,n}^j$ and corresponding energy eigenvalues ε_j, which give the total energy of the electron, are obtained by diagonalising the Hamiltonian matrix. The elements used to construct the Schrödinger equation in matrix form between basis states with quantum numbers (r', n') and (r, n) is given by

$$\begin{aligned} \langle r', n'|\hat{H}|r, n\rangle = {} & \left(n + \tfrac{1}{2}\right)\hbar\omega_c\,\delta_{r'r}\,\delta_{n'n} + \frac{\pi^2 r^2\hbar^2}{2m^* w^2}\,\delta_{r'r}\,\delta_{n'n} + eF\langle r'|\left(\tfrac{w}{2} - x\right)|r\rangle\,\delta_{n'n} \\ & + \frac{e^2 B_z^2}{2m^*}\langle r'|x^2|r\rangle\,\delta_{n'n} - \frac{e^2 B_z B_x}{m^*}\langle r'|x|r\rangle\langle n'|\bar{z}|n\rangle \end{aligned} \tag{25}$$

It can be shown using the recurrence relation for the Hermite polynomials that

$$\langle n'|\bar{z}|n\rangle = \left(\frac{(n+1)\hbar}{2m^*\omega_c\cos\theta}\right)^{\frac{1}{2}}\delta_{n',n+1} + \left(\frac{n\hbar}{2m^*\omega_c\cos\theta}\right)^{\frac{1}{2}}\delta_{n',n-1} \tag{26}$$

Since it is not possible to expand the wavefunction in terms of the full infinite expansion, the basis functions are cut off at a finite value. The value is sufficiently large that the addition of extra states has very little effect on the eigenvalues, and also the overall wavefunctions of the system. Two-dimensional contour maps of electron density inside the well are obtained by summing the contribution of each basis function in the finite expansion and squaring the result to obtain $|\psi(x,z)|^2$. Repeating this method at regular points throughout the well gives a complete picture of the electron position probability density distribution in the x-z plane of the potential well.

Chapter 5

Results

The results presented in this chapter are for calculations on the classical motion of an electron confined to the infinite potential well for the cases of a perpendicular magnetic field at $\theta = 0°$, and a tilted magnetic field tilted at $\theta = 20°$ to the barrier walls. The corresponding quantum mechanical eigenfunctions of the electron are also described for the tilted magnetic field case. The width of the potential well in all cases is taken to be $w = 120$ nm, with an electric field of strength $F = 5.35 \times 10^5$ Vm^{-1}, and a magnetic field $B = 11.4$ T applied to the well. To simplify calculations, the mass of the electron is taken to be a constant value $m^* = 0.067\, m_e$, where m_e is the mass of a free electron. This corresponds to an average value of the electron mass in the conduction band of a GaAs semiconductor.

5.1 Classical motion of an electron in a magnetic field applied at $\theta = 0°$

When the magnetic field is applied perpendicular to the barriers the classical motion of the system is regular and generally quasi-periodic. This is illustrated in the Poincaré section shown in figure 9 performed at an energy $E = 110$ meV. It was generated by initiating 30 classical orbits from the emitter barrier with different combinations of velocity components. The Poincaré section was built up for a given orbit, by plotting the y and z components of the electron velocity for 500 collisions with the emitter barrier. The concentric circular sets of points are characteristic of quasi-periodic trajectories in integrable systems as explained in chapter 2. The circles depict the regular nested tori on which each electron trajectory moves along in phase space. This is also in agreement with the standard description of quasi-periodic motion given in chapter 2. Figure 10 illustrates the regularity of the electron motion in this case by plotting a typical electron trajectory in position space for 14 collisions with the emitter barrier, also at $E = 110$ meV. Between collisions with the walls, the electron executes cyclotron motion about the magnetic field direction due to the Lorentz force acting on the electron. This is shown clearly in the 3-dimensional plot in the

unrotated co-ordinate system in figure 10(a). The electron is also uniformly accelerated along the x-axis by the electric field, as clearly shown in the two-dimensional plot in figure 10(b). The motion in the untilted field regime is completely integrable resulting in completely stable and regular motion as expected.

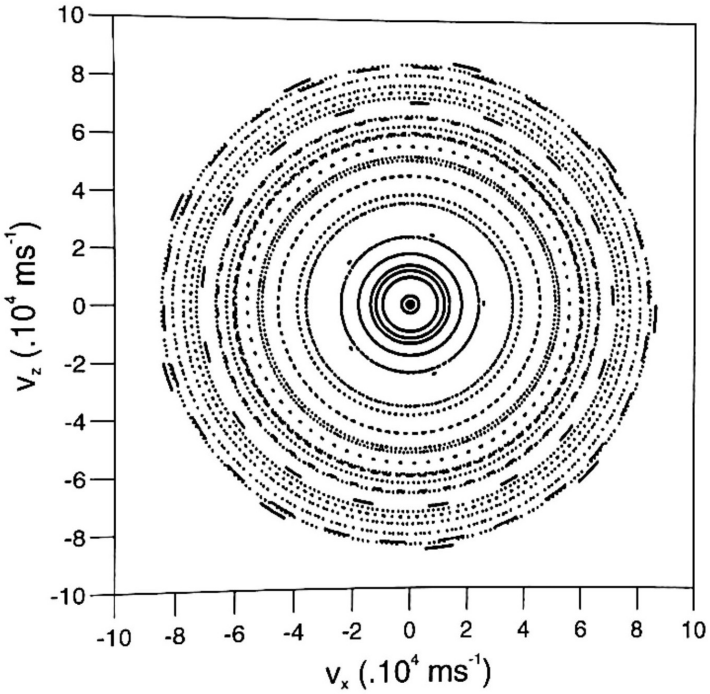

Figure 9: Poincaré section calculated for a range of starting velocities at energy $E =$ 110 meV in the untilted magnetic field regime.

5.2 Classical motion of an electron in a magnetic field applied at $\theta = 20°$

Tilting the magnetic field causes the electron to execute chaotic classical motion. Figure 11 shows a Poincaré section plotted for a single electron trajectory again with $E = 110$ meV. The plot shows a random scattering of points that is characteristic of strongly chaotic motion. The strongly chaotic nature of the electron in the tilted field regime is further displayed with the graphical projections of a typical electron trajectory, shown in figure 12. The orbit was calculated for only 10 collisions with the left-hand barrier. It is easily observable that the electron moves along a highly irregular path between the barriers,

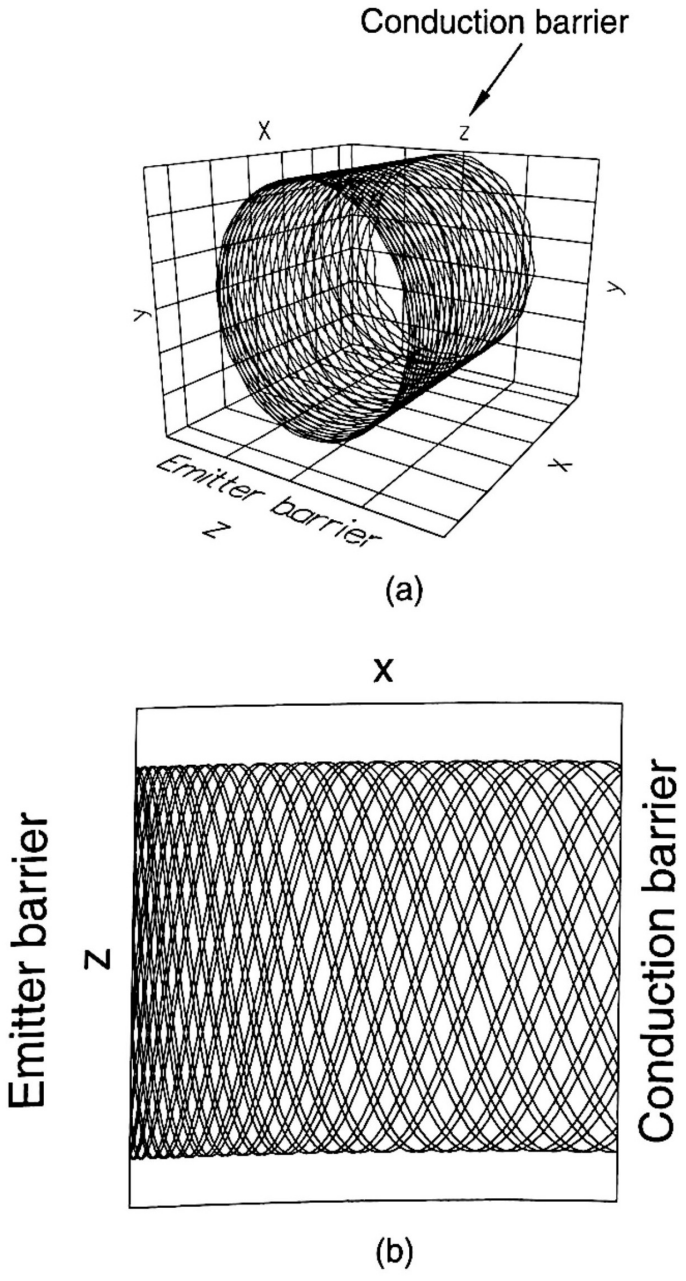

Figure 5.1 a. Classical cyclotron electron motion inside the potential well with the

Figure 10: a. Classical cyclotron electron motion inside the potential well with the magnetic field applied perpendicular to the barrier walls. b. Corresponding electron trajectory in the x-z plane.

gradually covering all the available area in the narrow channel along the magnetic field direction. The reason for this chaos is because tilting the magnetic field causes the cyclotron and longitudinal motion described previously to be mixed. This allows energy to be randomly transferred between the two types of motion on each collision with a barrier, therefore producing non-integrable chaotic motion. The degree of chaos exhibited by the electron is dependent on the tilt angle of the magnetic field. Consequently, increasing the tilt angle causes the electron to be more strongly chaotic.

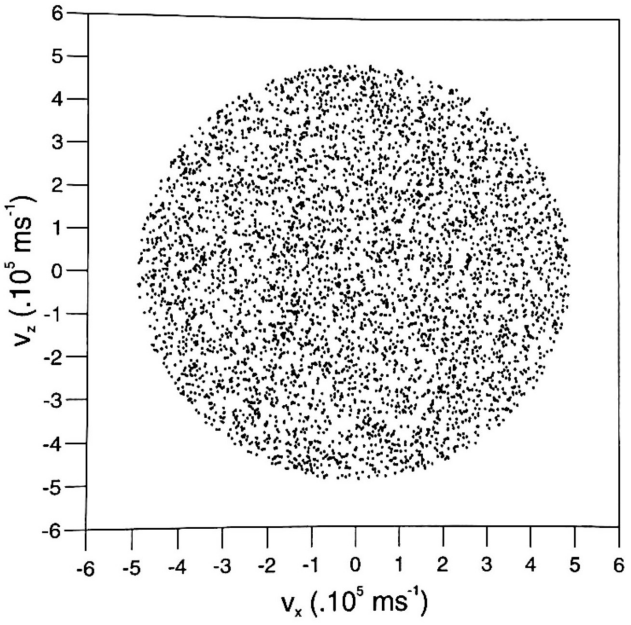

Figure 11: Poincaré section calculated for a chaotic trajectory at energy $E = 110$ meV in the tilted magnetic field regime.

Within the infinite number of chaotic trajectories that could take place for a given energy, there also exist a small number of periodic orbits for this system. Figure 13 shows projections of one such orbit that was found at energy $E = 96.16$ meV. The plots show the periodic orbit after 40 collisions with the emitter barrier. The orbit is unstable since only a very small perturbation is required to make the trajectory move off its distinct path and become highly irregular like that shown in figure 12. Periodic orbits with this particular shape occur at all energies up to 150 meV and is the most commonly found

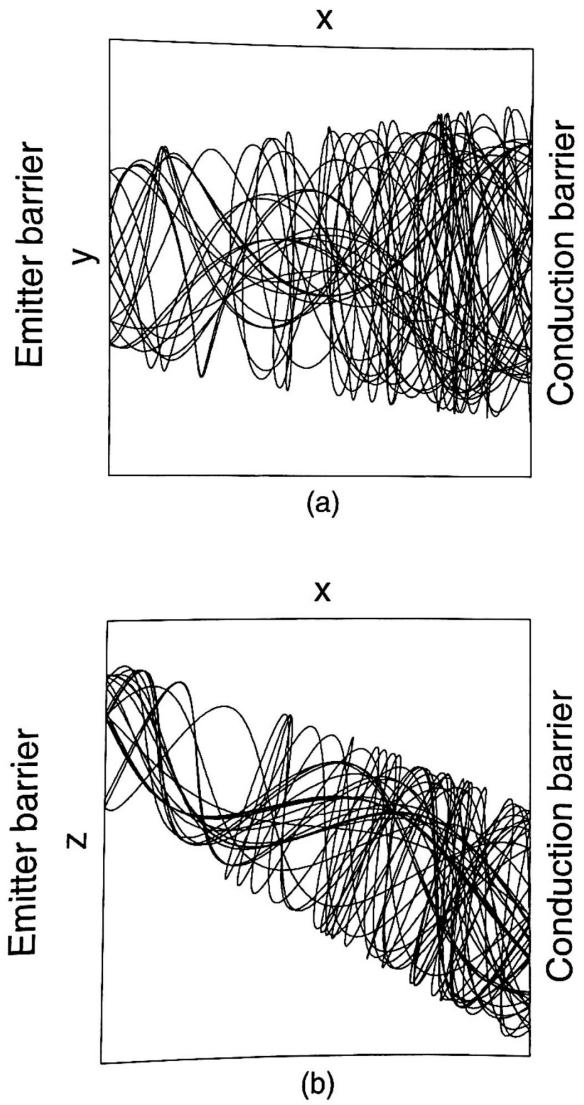

Figure 12: a. Strongly chaotic electron motion inside the well caused by tilting the magnetic field. b. Projection of the motion in the x-z plane.

unstable periodic orbit for this system up to electron energies of 150 meV.

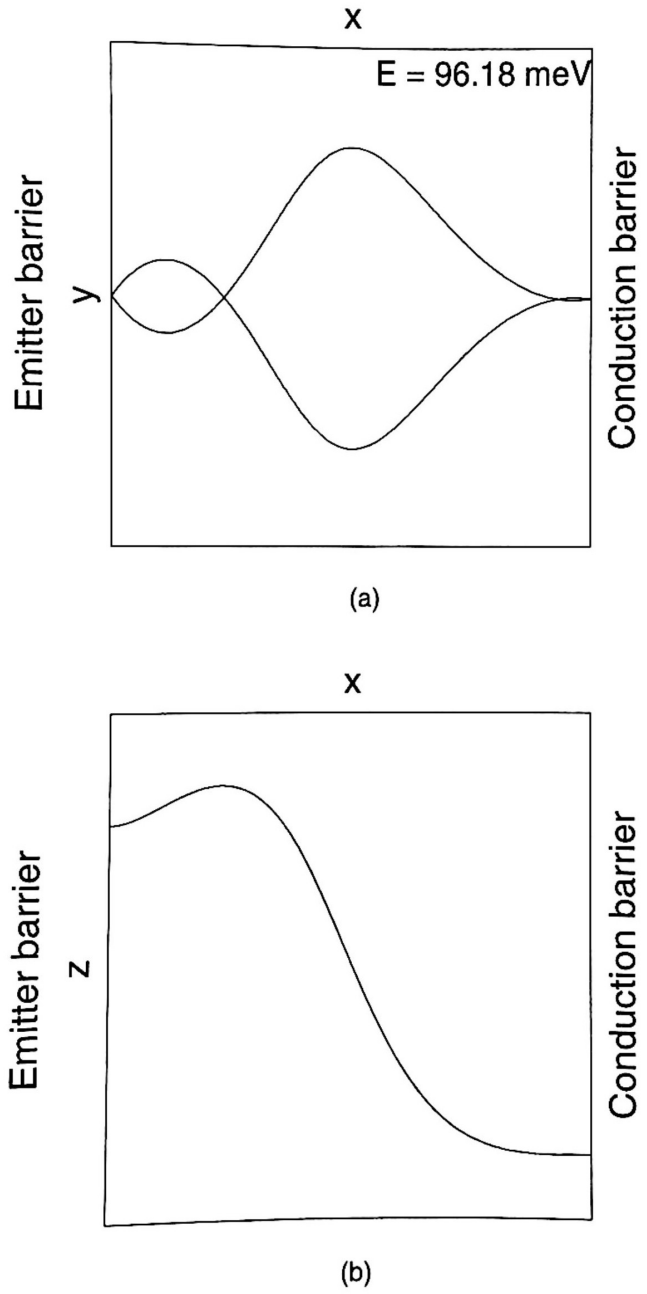

Figure 13: a. Trajectory of an unstable periodic orbit in the x-y plane. b. x-z projection of the periodic orbit.

At approximately $E = 150$ meV there is a transition point in which the trajectories in phase space change from being predominantly unstable to a mixture of stable and unstable orbits. Figure 14 depicts this transitionary energy range with Poincaré sections plotted for trajectories at three energy values. They illustrate the growth with increasing energy of a region of stability that is inaccessible to chaotic orbits, and consequently is devoid

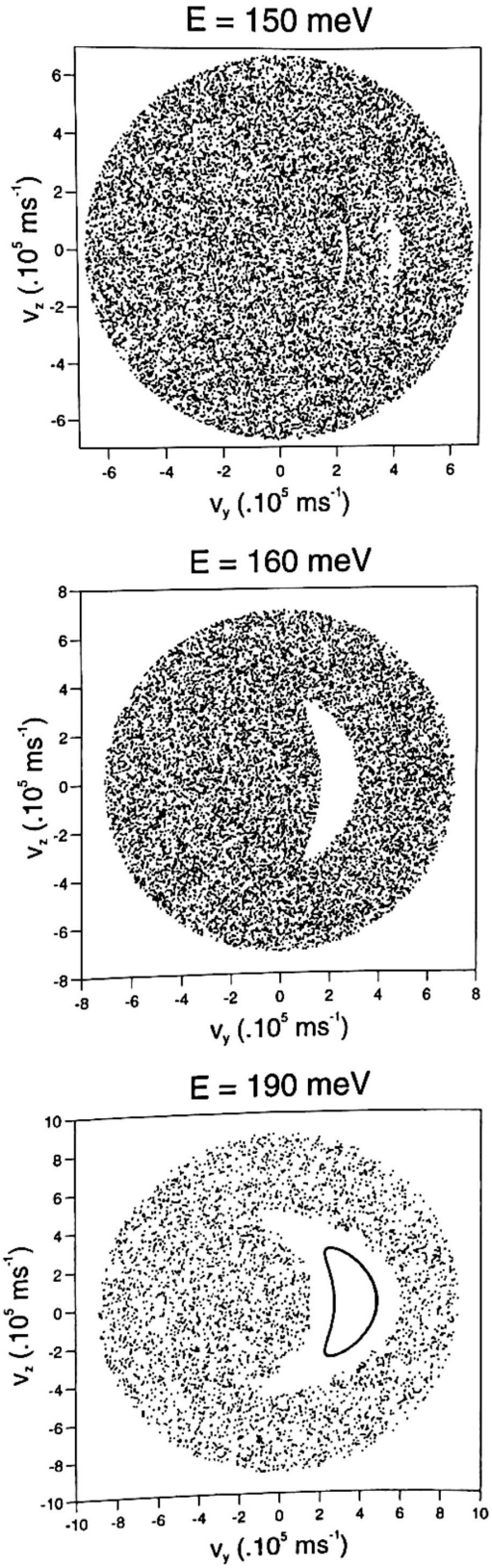

Figure 14: Poincaré sections showing the development of the region of stable electron motion with increasing energy.

of any points. Within this region, only quasi-periodic or periodic orbits can exist. The Poincaré section calculated at $E = 190$ meV shows one such quasi-periodic orbit located inside the considerably large stable region. This suggests that stable orbits of this system can be found for energies greater than 150 meV. An example of a typical stable periodic orbit for this system is shown Figure 15. The example shown for $E = 179.78$ meV was calculated for 400 collisions with the left-hand barrier. It appears that the orbit would remain almost exactly along this specific path for many more collisions if allowed, since there seems to be no observable deviance of the electron from the plotted path line. This is a clear indication of the stability of the orbit. This type of periodic orbit is the most likely candidate to scar quantum wavefunctions with energy greater than $E = 150$ meV.

The two types of periodic orbits discovered thus far are known as $[1, 1]$ periodic orbits since the electron makes a single collision with the conduction barrier before returning to the emitter barrier along the closed path. An example of a highly unstable periodic of type $[1, 2]$ is shown in figure 16. In this case, the electron collides with the conduction barrier twice before executing much more complicated motion before returning to the emitter barrier. Due to the rare occurrence of this periodic orbit it is expected that this kind would not be the cause of any scarring of electron wavefunctions inside the well.

5.3 Quantum wavefunctions of the well in the tilted magnetic field regime

Two-dimensional plots of electron probability density, $|\Psi|^2$, at various energy eigenvalues is shown in figure 17 with the magnetic field tilted at $\theta = 20°$. Since the quantum mechanics for the system is independent of the y-coordinate, all wavefunctions are plotted in the x-z plane. These represent typical eigenfunctions of the potential well and in general they show rather complex patterns of intermingled nodes and anti-nodes centred around the magnetic field direction. These states are termed 'unscarred' since there are no distinct topological features to suggest that anything but chaotic motion is being displayed by the electron inside the well.

Occurring at fairly regularly spaced intervals of energy and amongst the unscarred energy levels, there also exist wavefunctions that have a well defined line of probability

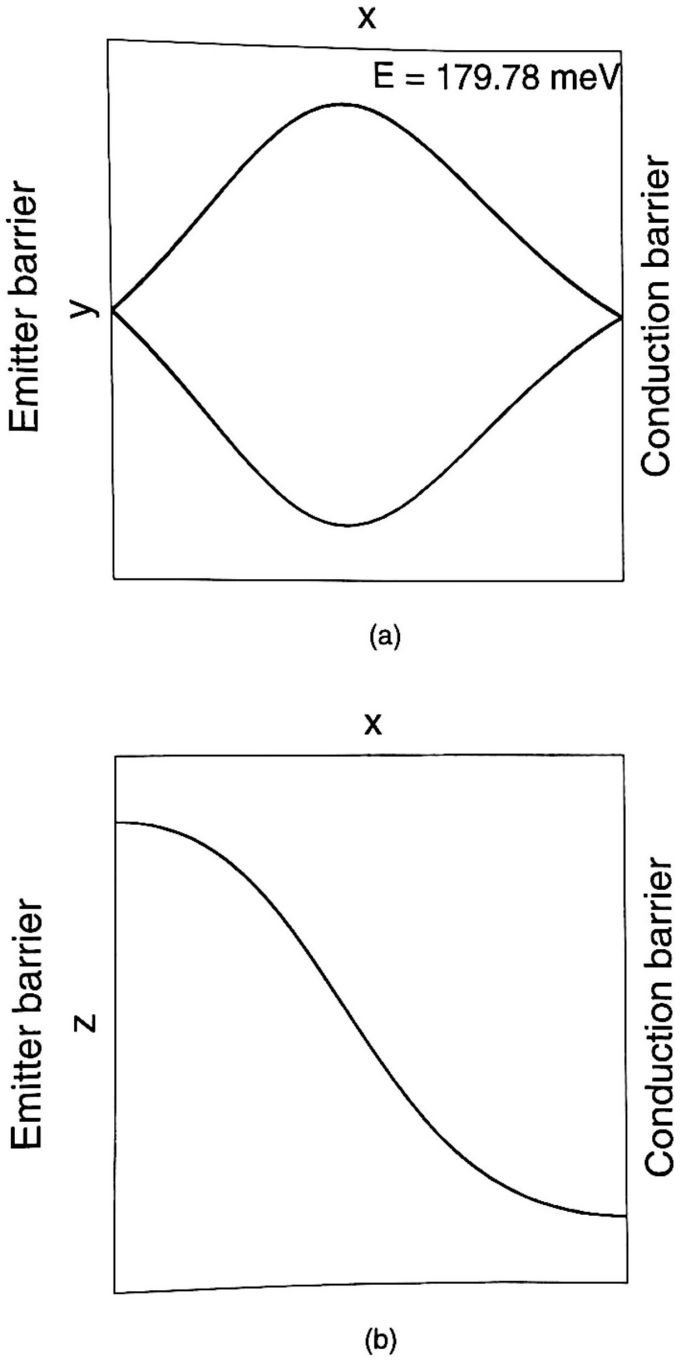

Figure 15: a. Trajectory of a stable periodic orbit of the system. b. x-z projection of the periodic orbit.

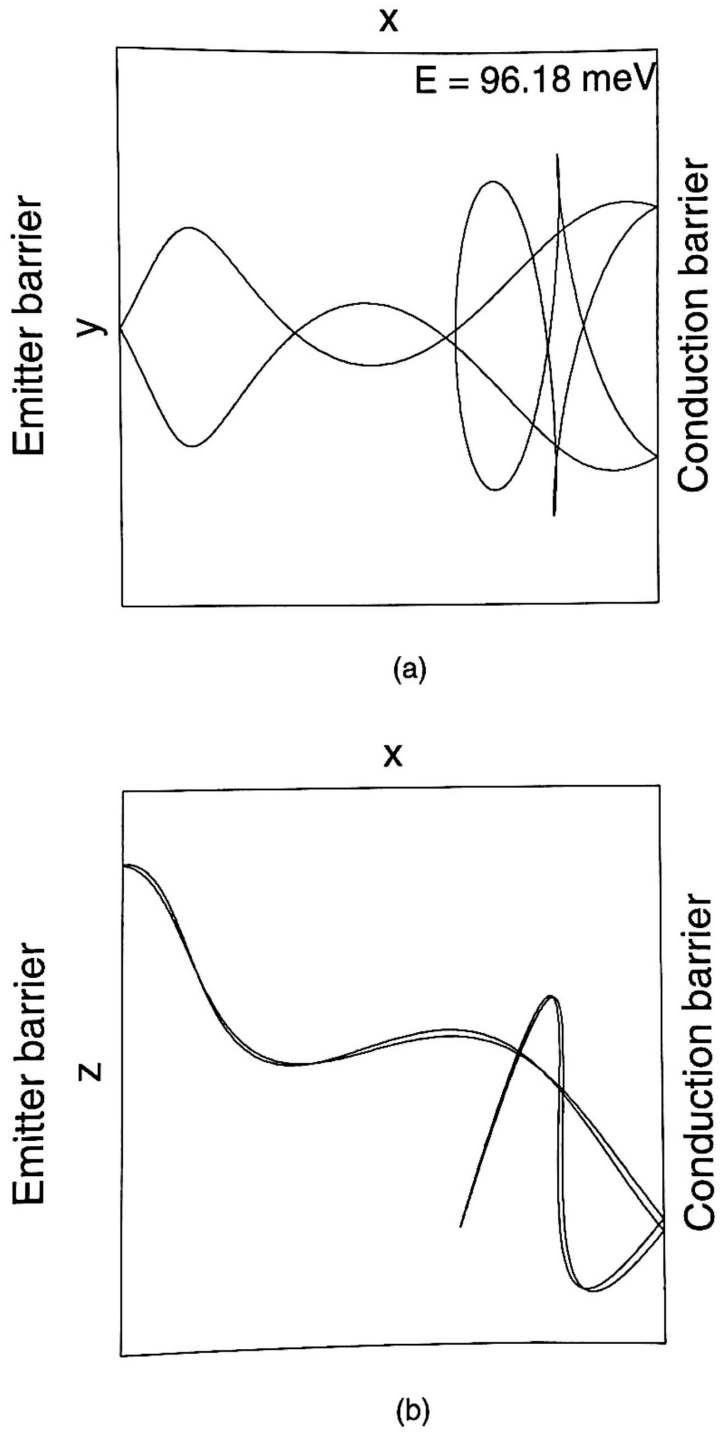

Figure 16: a. A highly unstable periodic orbit of the system. b. Projection in the x-z plane.

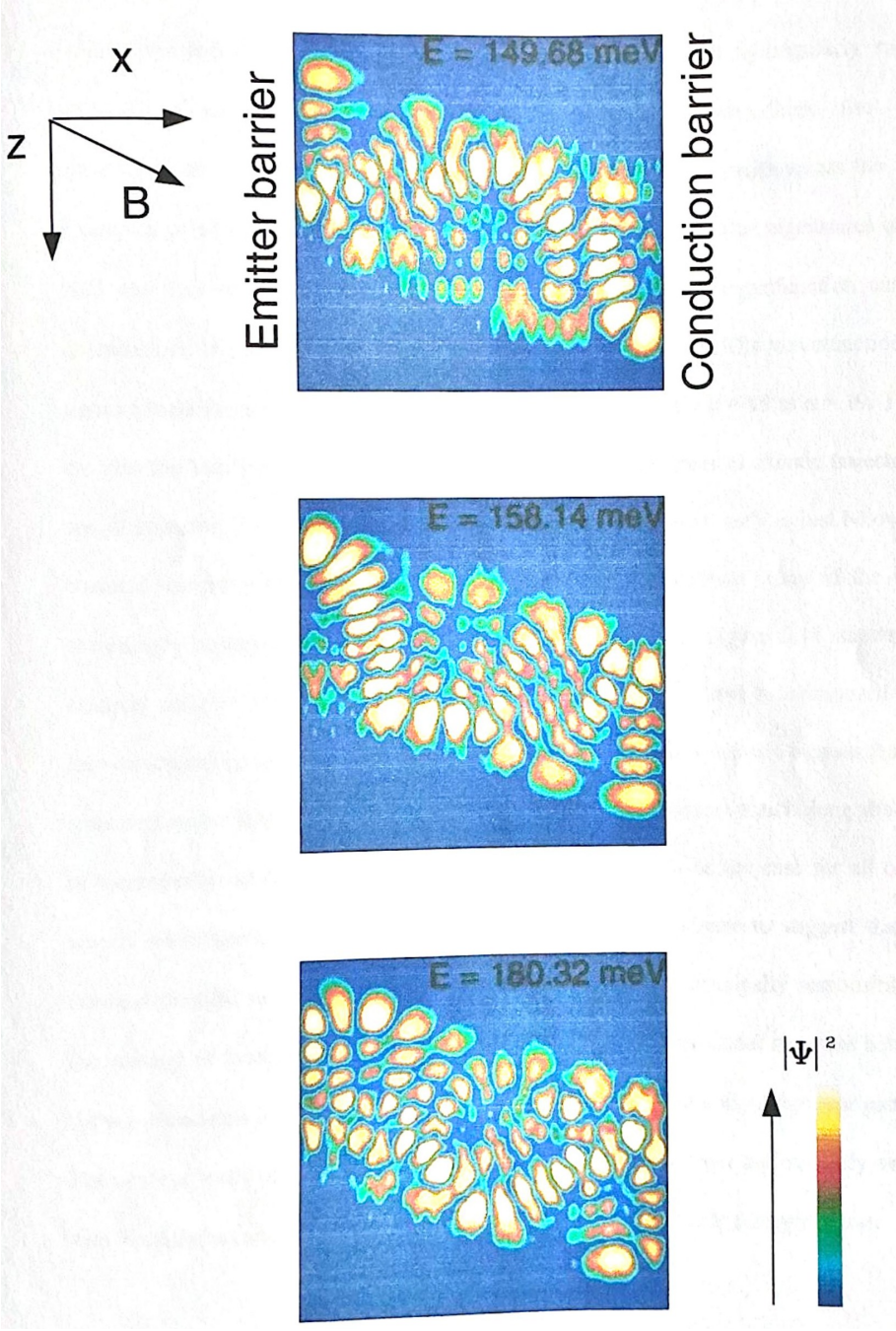

Figure 17: Electron probability density plots of 'unscarred' eigenfunctions of the potential well in a tilted magnetic field.

density peaks across the well. Examples of which are shown in figure 18. These completely distinct eigenstates of the well are 'scarred' wavefunctions of the system. Each scarred eigenfunction can be characterised in terms of the number, n, of anti-nodes in the plot. The wavefunctions in figure 18 are therefore consecutive scarred states of the well, for $n = 15$ to $n = 19$. These are also the last five scarred states in which the underlying classical chaotic trajectories are all unstable. The scarred wavefunction occurring at $E = 148.76$ meV is just below the classical transition point. Figure 19 shows the next three scarred states of the well, accordingly situated in the classically stable energy regime. Figure 20 shows the classical periodic orbits found earlier projected in the x-z plane and superimposed onto the corresponding scarred wavefunctions at the same energy.

It can easily be seen that the increased probability density associated with the scarring is concentrated along the path of the periodic orbit in the classical regime. This is found to be the case for all of the scarred wavefunctions calculated here. This gives strong evidence to suggest that the classical periodic orbits described in the previous section are principally responsible for the scarring of these quantum wavefunctions. The clarity of the nodal structure between the wavefunctions is reflected by the type of periodic orbits that underly the scar patterns. The contour plots of figure 19 appear to be much more distinct and strongly scarred than the plots shown in figure 18 which are scarred by unstable periodic orbits.

A different type of scarred wavefunction that consists of two channels of enhanced probability amplitude is found to occur in the system, as displayed in figure 21. This scar pattern occurs less frequently than those described previously. Only three occur within the energy range studied, observed at an average energy spacing of 90 meV. Such wavefunctions may be scarred by a rare type of periodic orbit that has eluded detection in this investigation, despite the fact that the wavefunction appears to be very strongly scarred.

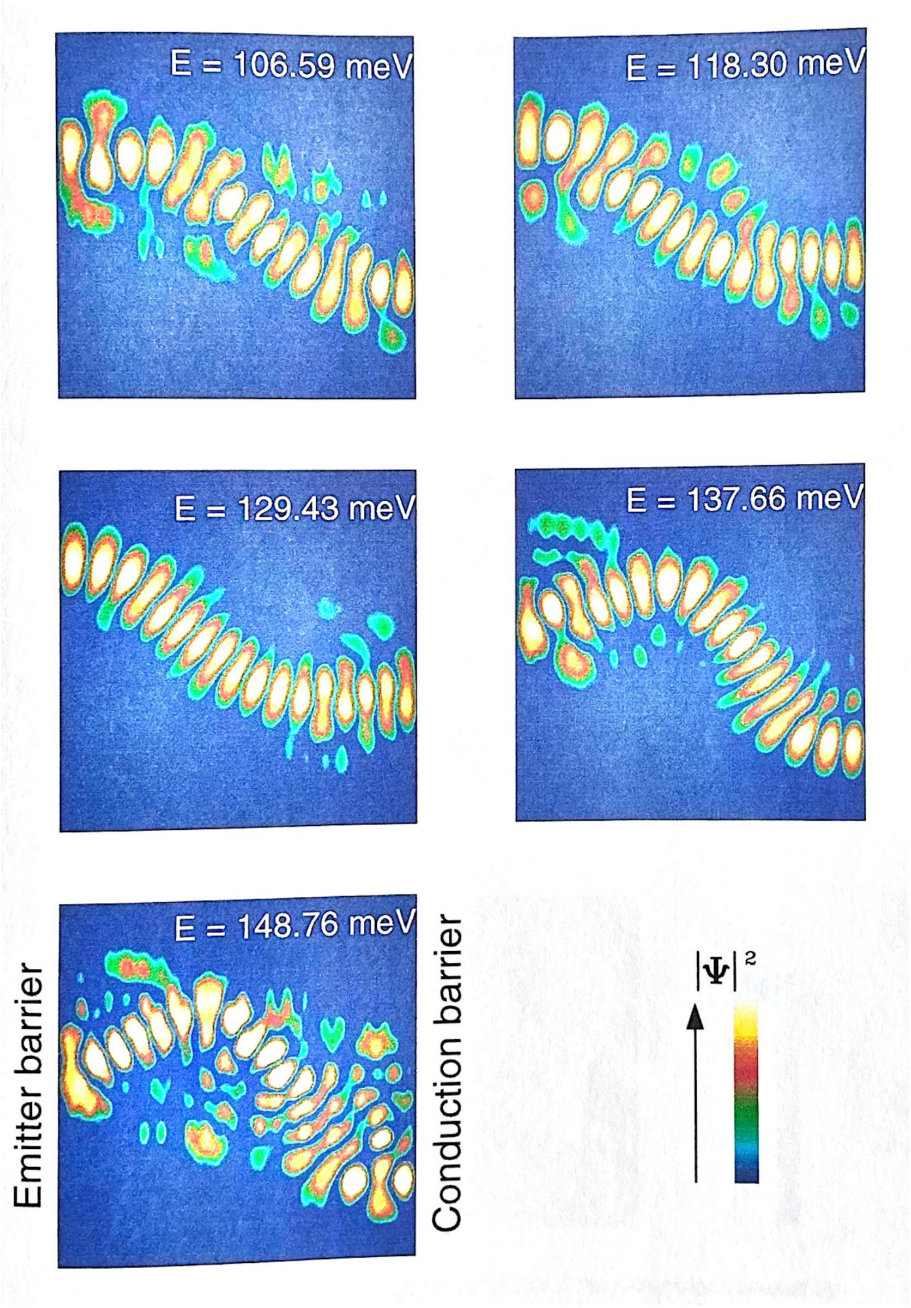

Figure 18: Examples of consecutive scarred eigenstates of the potential well.

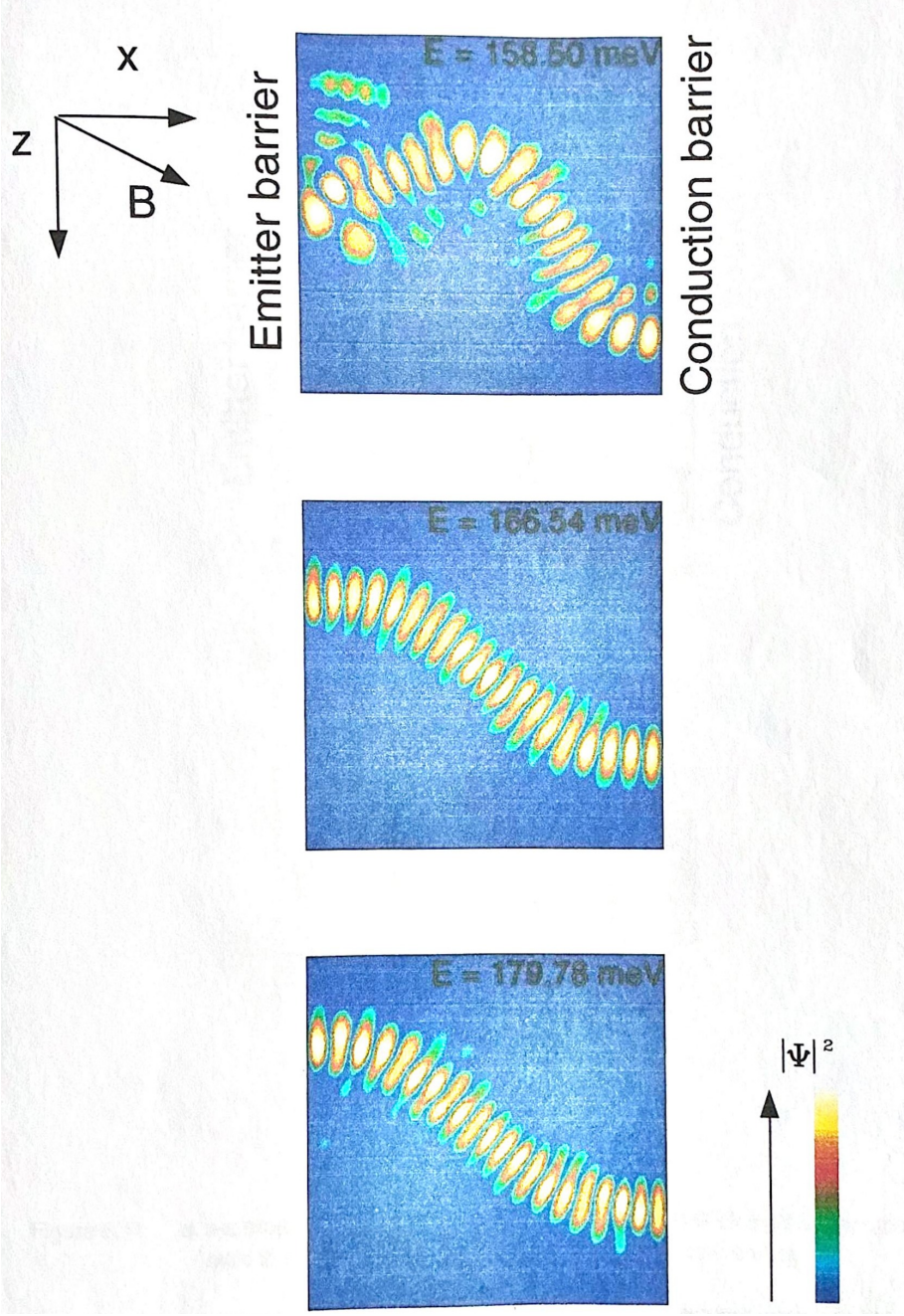

Figure 19: Probability density plots of scarred eigenfunctions caused by stable classical periodic orbits of the system.

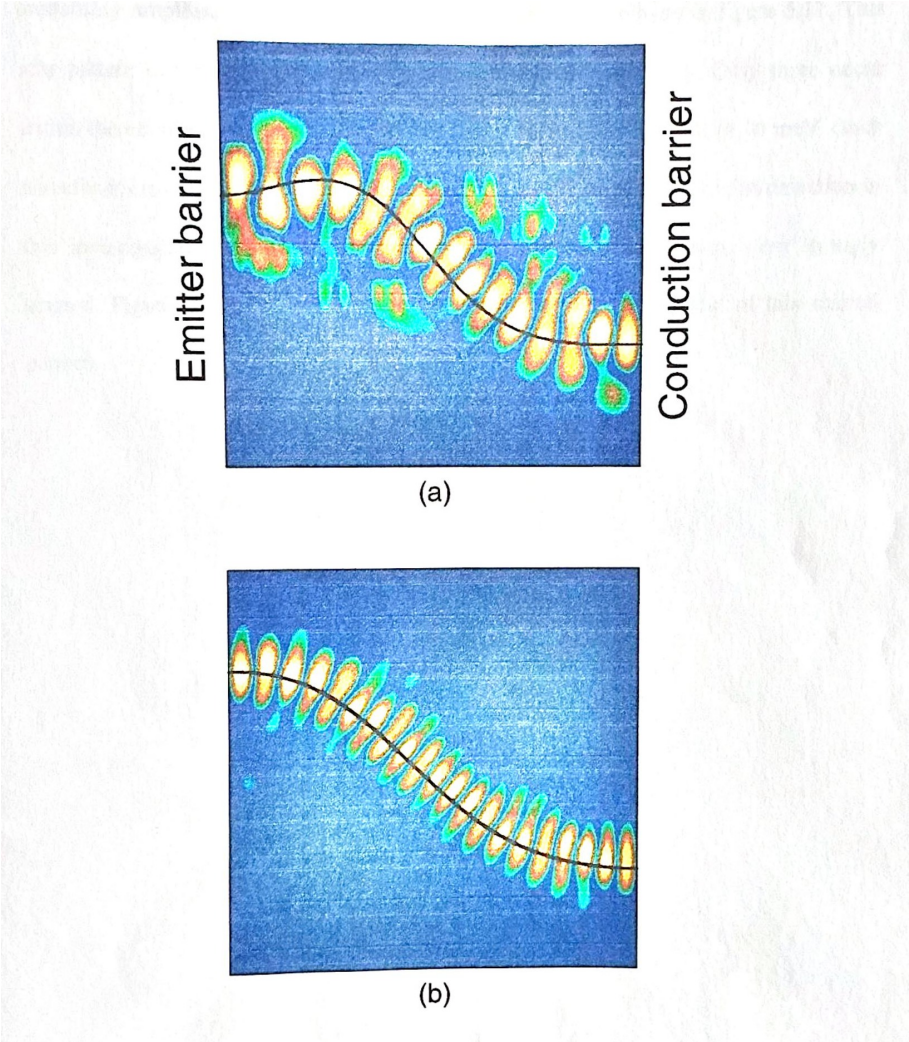

Figure 20: a. x-z projection of unstable periodic orbit at $E = 106.59$ meV superimposed onto the scarred electron wavefunction at the same energy.
b. Stable periodic orbit superimposed onto the scarred wavefunction at $E = 179.78$ meV.

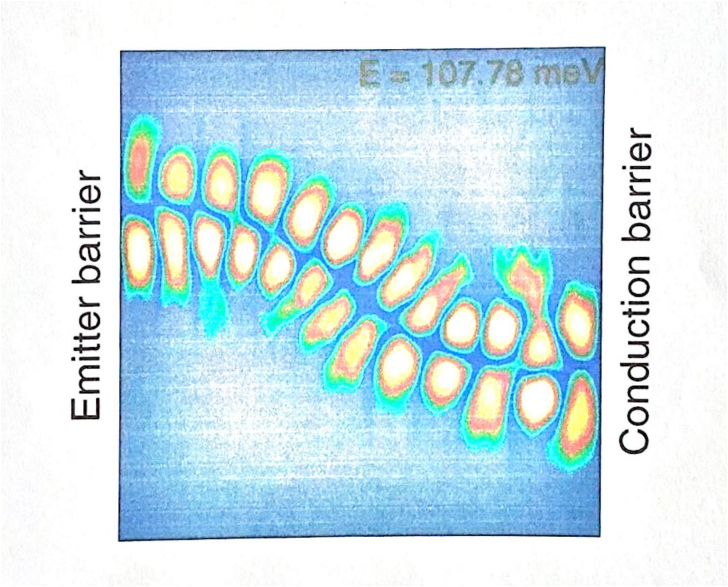

Figure 21: Wavefunction that appears to be scarred by two classical periodic orbits.

Chapter 6

Discussion

Determining the state of the electron as it collides with a barrier underpins the accuracy of the results for all of the classical calculations of the electron motion. A test of this is how well electron energy is conserved throughout a given orbit. Using the linear interpolation method the total energy changes by less than 0.08% for 500 collisions with the barriers. The method can be considered sufficiently accurate for determining the periodic orbits described here since the electron energy is fairly well conserved over a path consisting of 40 collisions with the emitter barrier. A polynomial interpolation is an obvious way of improving the collision process for orbits that require more accurate calculations.

In order to speed up calculations of quantum mechanical probability density distributions, the mass of the electron was taken to be a constant, m^*, corresponding to the effective electron mass in GaAs semiconductor structures. To ensure correspondence between the classical and quantum descriptions of the system the same value of the electron mass had to be employed in the classical calculations. A constant value for the effective mass of an electron can only be used if the conduction band in GaAs is assumed to be isotropic. This, however, is not the case in 'real' GaAs structures. The effective mass is actually dependent on the position of the electron inside the well and this is due to deviations from the usual parabolic nature of the conduction band. The change of effective mass is given by the relation

$$m^* = m_B\{1 + \alpha T(x)\} \tag{27}$$

where $m_B^* = 0.067\, m_e$ is the conduction band edge mass in bulk GaAs and $T(x)$ is the kinetic energy of the electron, which is dependent on the position of the electron along the x-axis. The constant, α, is a measure of the degree of non-parabolicity of the conduction band in GaAs, see P.B. Wilkinson. The change in shape of periodic orbits when including the band non-parabolicity factor was just observable for higher energy orbits, the change

being very small. Due to such insignificant deviations, it gave confidence in using the constant value for the effective mass especially when considering the added complications it would cause when evaluating the quantum probability density plots. Hence accurate representations of the wavefunctions of the quantum well can be obtained without including this factor.

It is only ever possible to expand the quantum mechanical Hamiltonian over a finite basis set as an approximation to the complete infinite expansion of states that span the wavefunction. Therefore the probability density plots produced in this project are accurate only up to a given energy. The value of this energy level and also the accuracy of the quantum mechanical results is obtained by testing the convergence of the energy eigenvalues to a constant value. This is done by plotting the basis set number against the energy levels of the system. It was revealed that energy levels up to 230 meV converge to constant values using 40 basis states in each of the x and z directions. Hence the eigenfunctions plotted here are only accurate up to 230 meV using a basis set size of 40 eigenstates. The accuracy of the results was verified further by observing what visible effect increasing the basis set size beyond 40 states has on the topology of the wavefunctions for the system. It was found that graphical plots of the electron probability density changed very little on increasing the basis set size beyond 40 states; the difference not warranting the substantial increase in computational time required to produce them. To investigate wavefunctions of higher energy a larger basis set size would clearly be needed.

The use of 40 basis functions requires the diagonalisation of a matrix with dimension 1600, since the summation is over quantum numbers n and r in each of the x and z directions respectively. It was found that the available Nag library routines were awkward in completing such a task due to the large size of the matrix, therefore another procedure was sought. The best available method involved using two Fortran algorithms taken from the book, 'Numerical Recipes in Fortran', [see Press *et al* (1992)]. To test the results given out using this method, the results for the eigenvalues and eigenvectors of a much smaller test matrix were compared with those obtained using a Nag routine that could handle the smaller sized test matrix. The values obtained for each method were found to agree completely.

Chapter 7

Conclusion

This investigation has studied a relatively simple system that consists of electron motion inside an infinite potential well subject to electric and magnetic fields. It is shown that the system becomes strongly chaotic in the classical regime when a magnetic field is tilted in a plane perpendicular to the confining barriers.

Two types of periodic orbits that most commonly occur for the system were found to 'scar' certain energy eigenstates in the quantum regime. This result illustrates further that classical chaos is intimately linked to the quantum mechanical regime through the periodic orbits of the classical system.

The remarkable phenomenon of wavefunction scarring in the system studied here affects individual eigenstates, leaving no trace of the scar pattern on adjacent energy levels. This is a unique property of the system since other studies of quantum chaos report that wavefunction scarring is a combined contribution from neighbouring eigenstates covering a range of energy levels [see Friedrich (1989)]. The cause of this intriguing property could provide a basis for future investigations.

Appendix A: Program Listings

Program cl_traj

```
Program cl_traj
implicit none
c-------------------------------------------------------------------------
c This program plots the classical trajectory of an electron confined within
c a 120nm wide quantum well subject to applied electric and untilted/tilted
c magnetic fields. Poincare sections are calculated and periodic orbits are
c also located.
c-------------------------------------------------------------------------
      integer count
      double precision t, const, omega, vdrift
      double precision cost, sint, theta, pi, F, B, ms
      double precision vx_dash, vy_dash, vz_dash
      double precision pxo, pyo, pzo, px, py, pz
      double precision vxo, vyo, vzo, vx, vy, vz
      double precision px_dash, py_dash, pz_dash
      double precision vx_cond, vy_cond, vz_cond
      double precision px_cond, py_cond, pz_cond
      double precision vx_emit, vy_emit, vz_emit
      double precision px_emit, py_emit, pz_emit
      double precision vxo_dash, vyo_dash, vzo_dash
      double precision pxo_dash, pyo_dash, pzo_dash
      double precision pxbfem, pzbfem, t_emit, vx_dash_em
      double precision pxbfco, pzbfco, t_cond, vx_dash_co
      double precision delta_vy, delta_vz, delta
      double precision vy_si, vz_si
      logical done
      parameter(theta=20.0d00, pi=3.14159265359d00)
```

```
      parameter(F=7.852265d-07, B=2.0078317178d-03, ms=0.067)
c-------------------------------------------------------------------------
c Equations that describe electron velocity components in the rotated
c coord system at time t
c-------------------------------------------------------------------------
      vx_dash(t)= 2*const*t + vxo_dash
      vy_dash(t)=(vyo_dash-vdrift)*cos(omega*t)
     +           -vzo_dash*sin(omega*t)+vdrift
      vz_dash(t)= (vyo_dash-vdrift)*sin(omega*t)+vzo_dash*cos(omega*t)
c-------------------------------------------------------------------------
c Equations describing electron velocity in the unrotated coord system
c at time t
c-------------------------------------------------------------------------
      vx(t)=cost*vx_dash(t)-sint*vz_dash(t)
      vy(t)=vy_dash(t)
      vz(t)=cost*vz_dash(t)+sint*vx_dash(t)
c
      cost=cos(theta*pi/180)
      sint=sin(theta*pi/180)
      const=F*cost/(2*ms)
      omega=B/ms
      vdrift=F*sint/B
c-------------------------------------------------------------------------
c Initialise position and velocity components.
c-------------------------------------------------------------------------
      vyo = 0.0028
      vxo = 0.0048462173434
      vzo = 0.000
      pxo = 0.0d00
      pyo = 0.0d00
      pzo = 0.0d00
```

```
c-------------------------------------------------------------------------
      vxo_dash = vxo*cost + vzo*sint
      vyo_dash = vyo
      vzo_dash = vzo*cost - vxo*sint
      pxo_dash = pxo*cost + pzo*sint
      pyo_dash = pyo
      pzo_dash = pzo*cost - pxo*sint
      open(1,file='cha_traj', status='unknown')
      open(2,file='veln.150',access='append',status='unknown')
c
      count = 0
 5    t=0.0d00
      done = .false.
c-------------------------------------------------------------------------
c Plot electron position in the well using the integrated equations of motion
c-------------------------------------------------------------------------
 10   if (.not.done) then
        px_dash = const*t**2+vxo_dash*t+pxo_dash
        py_dash = (vz_dash(t)-vzo_dash)/omega+vdrift*t+pyo_dash
        pz_dash =-(vy_dash(t)-vyo_dash)/omega+pzo_dash
c
c----------Rotate back into original coordinate system-----------
c
        px = px_dash*cost - pz_dash*sint
        py = py_dash
        pz = pz_dash*cost + px_dash*sint
c
      if (t.eq.0.0.and.vx(t).gt.0.0d00) then
        vxo = vx(t)
        vyo = vy(t)
        vzo = vz(t)
```

```
      end if
c
c     write(1,30)  px, py, -pz
c-------------------------------------------------------------------------
c Increment time in intervals of 1 or 0.01 when the electron gets closer
c than 1/20W (w=barrier width)
c-------------------------------------------------------------------------
        if (px.le.0.005d00.and.vx(t).lt.0.0d00.
     +      or.px.gt.0.995d00.and.vx(t).gt.0.0d00)then
          t = t + 0.01d00
```

(Program listing continues... see original document for full source of `cl_traj`, `qu_mat`, and `wav_fn` programs with subroutines `tred2`, `tqli`, `eigsrt`, and helper functions `pythag`, `herm`, `fact`, `pwr`.)

References

1. Arnold, V.I. *Mathematical Methods of Classical Mechanics* (Springer, New York, 1989)

2. Berry, M.V. *J. Phys. A* **10**, 2083 (1977)

3. Berry, M.V. & Tabor, M. *Proc. Roy. Soc. London A* **356**, 375 (1977)

4. Bunimovich, L.A. *Comm. Math. Phys.* **65**, 295 (1979)

5. Friedrich, H. & Wintgen, D. *Phys. Rep.* **183**, 37 (1989)

6. Fromhold, T.M., Fogarty, A., Eaves, L., Sheard, F.W., Henini, M., Foster, T.J., Main, P.C. & Hill G. *Phys. Rev. B* **51**, 18029 (1995)

7. Goldstein, H. *Classical Mechanics* (Addison-Wesley, 1990)

8. Gutzwiller, M.C. *J. Math. Phys.* **12**, 343 (1971)

9. Gutzwiller, M.C. *Chaos in Classical and Quantum Mechanics* (Springer-Verlag, Berlin, 1990)

10. Heller, E.J. *Phys. Rev. Lett.* **53**, 1515 (1984)

11. Press, W.H., Teukolsky, S.A., Vetterling, W.T. & Flannery, B.P. *Numerical Recipes in Fortran* (Cambridge University Press, 462–474, 1992)

12. Tabor, M. *Chaos and Integrability in Nonlinear Dynamical Systems* (Wiley, New York, 1989)

13. Wilkinson, P.B., Fromhold, T.M., Eaves, L., Sheard, F.W., Miura, N., & Takamasu, T. *Nature* **380**, 608 (1996)

14. Wilkinson, P.B. *Quantum Chaos in Resonant Tunnelling Diodes* (Doctoral Thesis, The University of Nottingham, 1997)